Langmuir

Article

pubs.acs.org/Langmuir

Synthesis of Optically Active Regioregular Polythiophenes and Their Self-Organization at the Air−Water Interface

Yuko Takeoka,* Fumihiko Saito, and Masahiro Rikukawa*

Department of Materials and Life Sciences, Sophia University, 7-1 Kioi-cho, Chiyoda-ku, Tokyo 102-8554, Japan

Supporting Information

ABSTRACT: Regioregular polythiophenes containing an optically active substituent in the third position of the thiophene ring, *head-to-tail* poly(3-[2-((*S*)-1-methyloctyloxy)-ethyl]thiophene)s (*HT*-P(*S*)MOETs), were synthesized using highly reactive zinc. For comparison, *HT*-P(*R*)MOET and achiral *HT*-P(±)MOET also were synthesized from *R*-type monomers and racemic monomers, respectively. The *HT*-PMOET possessed greater than 95% *head-to-tail* coupling with a weight-average molecular weight (M_w) between 1.96×10^4 and 2.94×10^4. The polymers were characterized using ^{1}H and ^{13}C NMR, optical rotatory power measurements, circular dichroism (CD), and UV−vis spectroscopy. X-ray diffraction patterns of the cast films demonstrated that regioregular *HT*-PMOET possessed a strong tendency to self-assemble into highly ordered, crystalline structures. The *HT*-P(*S*)MOET and *HT*-P(*R*)MOET showed strong Cotton effects, while *HT*-P(±)MOET showed very weak Cotton effects. The presence of a circular dichroism effect indicated that the side chain chirality induced optical activity in poly(thiophene) main chains. The monolayer formation of *HT*-PMOET spread on the water surface was characterized using a pressure−area (π−A) isotherm. The molecular areas of *HT*-P(*S*)MOET and *HT*-P(*R*)MOET molecules on the water surface were 33.5 and 32.9 Å^2, respectively, at 10 °C, which were larger than that of *HT*-P(±)MOET (27.9 Å^2), suggesting that optically active *HT*-PMOET expanded because of the chiral repulsion between side chains. Multilayer films of *HT*-PMOET were prepared by repeating horizontal deposition of the monolayer on the water surface. The multilayer films of optically active *HT*-PMOET obtained showed stronger Cotton effects than did the cast films. In addition, electrical conductivities of *HT*-PMOET multilayer films were superior to those of spin-coated films. *Head-to-tail* poly(3-[2-((*S*)-1-methylpropyloxy)ethyl]thiophene) (*HT*-P(*S*)MPET), which contained shorter side chain lengths compared to *HT*-P(*S*)MOET, also was synthesized. The CD intensities of *HT*-P(*S*)MPET multilayer films were smaller than those of *HT*-P(*S*)MOET multilayer films, suggesting that the optically active side-chain length is critically important to the optically active self-assembly.

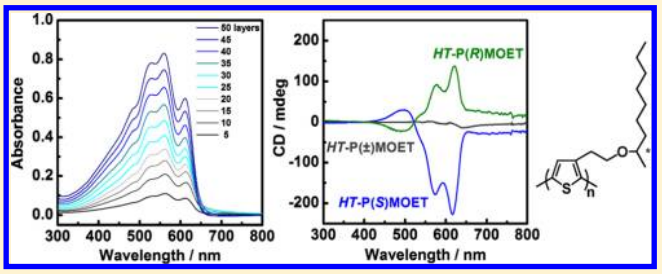

INTRODUCTION

Polythiophene and its derivatives have attracted considerable interest as conducting polymers because of their excellent electro-optical properties, good solubility, and environmental stability.[1,2] Their chemical versatility allows the use of various monomer building blocks and has led to the development of numerous polythiophene derivatives with transformable properties applicable to light-emitting diodes (LEDs),[3−6] photovoltaic cells,[7,8] organic field-effect transistors (OFETs),[9−11] and sensors.[12] Modification of polythiophenes using side chain functionalization provides a variety of nanostructures and electronic properties. For example, polythiophene derivatives containing optically active side chains exhibit the unique behavior of macromolecular self-assembly into helical aggregates that possess unique optical properties such as circular dichroism (CD) and circular polarized luminescence in the visible region.[13−17] To evaluate and enhance these properties for conducting polymers, the preparation of structurally homogeneous materials is important. The recent development of regioregular 3-substituted polythiophene offers a new direction for molecular engineering research.[18,19] These regiochemical arrangements provide an opportunity to understand the relationship between the structure and the properties of conducting polymers with enhanced electrical and optical properties. The electrical and optical properties of these polymers, based on conjugated systems, strongly depend on their nanostructural organization, which can be controlled by the introduction of regioregularity. For example, the hole mobility of regioregular poly(3-alkylthiophene) is greater than that of the regiorandom polymer by 1 order of magnitude.[20] The electrical and optical properties of conjugated polymers can be determined by their solid-state morphology, which depends on interchain conformation and the resulting interpolymer interactions. Therefore, researchers have focused on precise control of the molecular organization of polythiophenes in the film state to improve their properties and explore potential applications of these materials.[21] In most cases, conventional solution casting and spin-coating methods,

Received: April 25, 2013
Revised: May 24, 2013

   dx.doi.org/10.1021/la4015527 | *Langmuir* XXXX, XXX, XXX−XXX

which offer very little control of the molecular organization of the polymers, have been used to prepare polymer films. Consequently, a disordered structure often is transferred to the solid state during conventional film processing, making long-range ordering difficult to achieve without specific postprocessing.

The Langmuir−Blodgett (LB) technique offers a unique approach for application of ordered ultrathin films with well-defined architecture.[22−27] Application of the LB technique to conjugated polymers has produced various electrical and optical ultrathin film devices including field-effect transistors and LEDs. Polymeric materials suitable for the LB technique must be made amphiphilic by introducing an ionic or polar side or main chain to prepare a spreading monolayer at the air−water interface. Therefore, fully hydrophobic hydrocarbon-based polymers cannot form stable monolayers on water.[28] For polythiophene derivatives, regioregular poly(3-alkylthiophene)s form stable monolayer films as a result of rigid polymer main chains that direct spreading on the water surface.[29] However, the area per molecule of regioregular poly(3-alkylthiophene) films is relatively small compared with the ideal values and depends on preparation conditions. These results suggest that regioregular poly(3-alkylthiophene)s tend to aggregate because of strong self-organizing properties. To obtain ideal spread monolayers of regioregular poly(3-alkylthiophene), various supporting materials can be added to the polymer, such as liquid crystal molecules.[30] These LB films can be fabricated from mixed monolayers containing stearic acid and regioregular poly(3-alkylthiophene).[31,32] This novel approach results in well-defined and controllable molecular architecture with desirable optical and electrical properties. Moreover, highly ordered LB films of a regioregular chiral polythiophene, *head-to-tail* poly(3-[2-((S)-2-methylbutoxy)ethyl]thiophene) (*HT*-P(*S*)MBET), could be obtained without using stearic acid as an amphiphilic molecule.[33] Thus, LB manipulation of chiral polythiophene having a longer side chain than *HT*-P(*S*)MBET was demonstrated to be effective for monolayer formation. Furthermore, enhanced chiral, optical, and electrical properties were characterized.

EXPERIMENTAL SECTION

Materials. (*S*)-(+)-, (*R*)-(−)-2-Nonanol, (*S*)-(+)-butanol, iron(III) chloride, tetrahydrofuran (THF, for organic synthesis), acetonitrile (for organic synthesis), and 1,1,1,3,3,3-hexamethyldisilazane were purchased from Wako Pure Chemicals and used without further purification. Rieke Zn* (Zn*, Rieke Metals Inc., 5 wt % THF solution) was used without further purification. Pyridine was purchased and purified by distillation over potassium hydroxide. Hexane, *N*,*N*-dimethylformamide (DMF), and chloroform were purchased and purified by conventional methods. Diethyl ether was purchased and purified by distillation, followed by drying with $CaCl_2$ and Drynap. 2-(3-Thienyl)ethanol was purified by vacuum distillation. *p*-Toluenesulfonyl chloride was purified by recrystallization from diethyl ether.

Monomer Syntheses. *(S)-(+)-2−1-Methyloctyl p-Toluenesulfonate [(S)MOT].* *p*-Toluenesulfonyl chloride (4.69 g, 2.46×10^{-2} mol) was added slowly to a dry pyridine (9.00 g, 1.13×10^{-1} mol) solution of (*S*)-(+)-2-nonanol (3.00 g, 2.09×10^{-2} mol) in an ice bath. The reaction mixture was stirred for 20 h at 5 °C under nitrogen. The solution was extracted with diethyl ether, and the organic layer washed with 18 wt % hydrochloric acid and dried over anhydrous K_2CO_3/$MgSO_4$. After the solvent was evaporated, the residue was purified using column chromatography on Wakogel with hexane−diethyl ether (6:1, *v*/*v*) as the eluent to give 5.78 g (92.8%) of (*S*)MOT as colorless oil.[34] $[\alpha]_{589}$: +4.61°. IR (KRS, cm^{-1}): 2929 (s, νC−H), 2858 (s, νC−H), 1599 (w, νC═C), 1462 (m, δC−H), 1364 (w, νC-SOO-OC), 1177 (m, νCOC), 1097 (m, νCOC), 914 (w, δC−H), 815 (m, νC−H). ^{1}H NMR ($CDCl_3$): 7.79 (d, 2H), 7.32 (d, 2H), 4.60 (m, 1H), 2.44 (s, 1H), 1.38−1.63 (m, 2H), 1.11−1.27 (m, 15H), 0.87 (t, 3H). ^{13}C NMR ($CDCl_3$): 144.36, 134.65, 129.69, 127.72, 80.73, 36.51, 31.68, 29.09, 29.06, 24.87, 22.74, 21.61, 20.87, 14.07. EIMS: *m*/*z* = 298 (M^+), 126 ($CH_3CH_2C_7H_{15}^+$). Anal. Calcd for $C_{16}H_{26}O_3S$: C, 64.39; H, 8.78. Found: C, 64.43; H, 8.51.

3-[2-((S)-(+)-1-Methyloctyloxy)ethyl]thiophene [(S)MOET]. 2-(3-Thienyl)ethanol (1.80 g, 1.41×10^{-2} mol) and potassium hydroxide (1.31 g, 2.34×10^{-2} mol) were dissolved in THF (10 mL) and refluxed for 3 h. A THF solution (6 mL) of (*S*)MOT (4.01 g, 1.34×10^{-2} mol) then was added dropwise over 30 min. The reaction mixture was refluxed for 17 h, extracted with diethyl ether, and dried over anhydrous $MgSO_4$. After the solvent was evaporated, the residue was purified using column chromatography on a Wakogel with hexane−diethyl ether (10:1, *v*/*v*) as the eluent to give 1.80 g (52.8%) of (*S*)MOET as pale yellow oil.[34] $[\alpha]_{589}$: −3.07°. IR (KRS, cm^{-1}): 2956 (s, νC−H), 2927 (s, νC−H), 2856 (s, νC−H), 1466 (m, δC−H), 1372 (w, δC−H), 1340 (w, νC═C), 1121 (m, νCOC), 1095 (m, νCOC), 855 (w, δC−H), 772 (m, νC−H). ^{1}H NMR ($CDCl_3$): 7.23 (d, 1H), 7.02 (s, 1H), 6.99 (d, 1H), 3.56−3.70 (m, 2H), 3.37 (m, 1H), 2.89 (t, 2H), 1.51 (m, 2H), 1.26−1.35 (m, 10H), 1.12 (d, 3H), 0.88 (t, 3H). ^{13}C NMR ($CDCl_3$): 139.57, 128.56, 125.05, 121.00, 75.69, 68.62, 36.69, 31.86, 31.20, 29.71, 29.32, 25.71, 22.68, 19.71, 14.12. EIMS: *m*/*z* = 254 (M^+), 126 ($CH_3CH_2C_7H_{15}^+$), 111 ($C_6H_7S^+$). Anal. Calcd for $C_{15}H_{26}OS$: C, 70.81; H, 10.30. Found: C, 70.40; H, 10.43.

2,5-Dibromo-3-[2-((S)-(+)-1-methyloctyloxy)ethyl]thiophene [DBr-(S)MOET]. Dibromination of (*S*)MOET was performed with *N*-bromosuccinimide (NBS) in DMF. (*S*)MOET (3.00 g, 1.18×10^{-2} mol) was dissolved in DMF (10 mL) in an ice bath. A DMF solution (50 mL) of NBS (4.61 g, 2.59×10^{-2} mol) was added dropwise into the (*S*)MOET solution over 45 min. After the reaction mixture was stirred for 24 h at 0 °C, the solution was extracted with diethyl ether (3 × 60 mL); the organic extracts were successively washed with water (2 × 60 mL), aq. $NaHCO_3$ (3 × 60 mL), and aq. NaCl (2 × 60 mL). The organic layer was dried over anhydrous $MgSO_4$. After the diethyl ether was evaporated, the residue was purified using column chromatography on a Wakogel with hexane−diethyl ether (4:1, *v*/*v*) as the eluent to give 4.85 g (99.7%) of DBr-(*S*)MOET as a yellow oil. $[\alpha]_{589}$: −3.94°. IR (KRS, cm^{-1}): 2954 (s, νC−H), 2930 (s, νC−H), 2852 (s, νC−H), 1538 (w, νC═C), 1467 (m, δC−H), 1375 (w, δC−H), 1342 (w, νC═C), 1124 (m, νCOC), 1098 (m, νCOC), 982 (w, νC−Br). ^{1}H NMR ($CDCl_3$): 6.88 (s, 1H), 3.47−3.63 (m, 2H), 3.38 (m, 1H), 2.79 (t, 2H), 1.55 (m, 2H), 1.26−1.39 (m, 10H), 1.12 (d, 3H), 0.88 (t, 3H). ^{13}C NMR ($CDCl_3$): 139.88, 131.59, 110.22, 108.87, 75.81, 67.00, 36.65, 31.86, 30.52, 29.70, 29.34, 25.55, 22.69, 19.66, 14.12. EIMS: *m*/*z* = 412 (M^+), 126 ($CH_3CH_2C_7H_{15}^+$). Anal. Calcd for $C_{15}H_{26}Br_2OS$: C, 43.71; H, 5.87. Found: C, 43.97; H, 5.94.

(R)-(−)-2−1-Methyloctyl p-toluenesulfonate [(R)MOT]. (*R*)MOT was prepared from (*R*)-(−)-2-nonanol in a manner identical to that for (*S*)MOT. Yield: 79.5%. $[\alpha]_{589}$: −3.94°. ^{1}H NMR ($CDCl_3$): 7.78 (d, 2H), 7.32 (d, 2H), 4.60 (m, 1H), 2.44 (s, 1H), 1.38−1.64 (m, 2H), 1.11−1.26 (m, 15H), 0.87 (t, 3H). ^{13}C NMR ($CDCl_3$): 144.35, 134.66, 129.68, 127.73, 80.73, 36.51, 31.68, 29.09, 29.06, 24.87, 22.74, 21.62, 20.87, 14.07. EIMS: *m*/*z* = 298 (M^+), 126 ($CH_3CH_2C_7H_{15}^+$). Anal. Calcd for $C_{16}H_{26}O_3S$: C, 64.39; H, 8.78. Found: C, 64.56; H, 8.85.

3-[2-((R)-(−)-1-Methyloctyloxy)ethyl]thiophene [(R)MOET]. (*R*)MOET was prepared from (*R*)MOT in a manner identical to that for (*S*)MOET. Yield: 61.6%. $[\alpha]_{589}$: +3.56°. ^{1}H NMR ($CDCl_3$): 7.24 (d, 1 H), 7.03 (s, 1H), 6.99 (d, 1H), 3.56−3.70 (m, 2H), 3.37 (m, 1H), 2.89 (t, 2H), 1.51 (m, 2H), 1.26−1.35 (m, 10H), 1.12 (d, 3H), 0.87 (t, 3H). ^{13}C NMR ($CDCl_3$): 139.58, 128.57, 125.05, 121.00, 75.70, 68.63, 36.70, 31.86, 31.21, 29.72, 29.32, 25.71, 22.69, 19.72, 14.12. EIMS: *m*/*z* = 254 (M^+), 126 ($CH_3CH_2C_7H_{15}^+$), 111 ($C_6H_7S^+$). Anal. Calcd for $C_{15}H_{26}OS$: C, 70.81; H, 10.30. Found: C, 70.97; H, 10.16.

2,5-Dibromo-3-[2-((R)-(-)-1-methyloctyloxy)ethyl]thiophene [DBr-(R)MOET]. DBr-(*R*)MOET was prepared from (*R*)MOET in a manner identical to that for DBr-(*S*)MOET. Yield: 82.3%. $[\alpha]_{589}$:

dx.doi.org/10.1021/la4015527 | *Langmuir* XXXX, XXX, XXX−XXX

Scheme 1. Syntheses of *HT*-PMPET and *HT*-PMOET

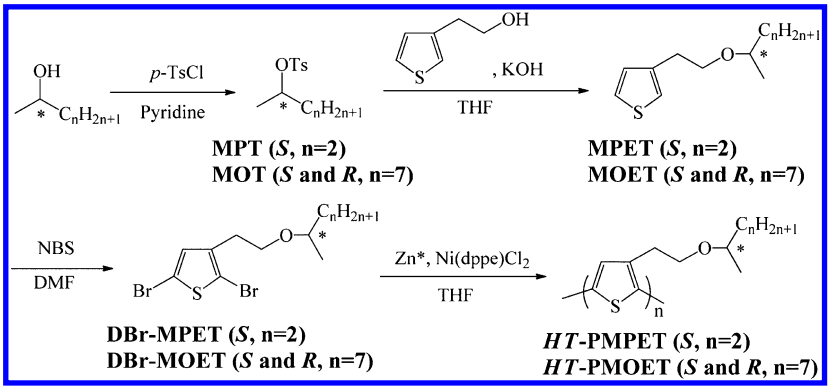

+2.63°. ^{1}H NMR ($CDCl_3$): 6.90 (s, 1H), 3.47−3.63 (m, 2H), 3.38 (m, 1H), 2.79 (t, 2H), 1.54 (m, 2H), 1.26−1.41 (m, 10H), 1.11 (d, 3H), 0.88 (t, 3H). ^{13}C NMR ($CDCl_3$): 139.88, 131.59, 110.22, 108.87, 75.81, 67.00, 36.65, 31.86, 30.52, 29.70, 29.34, 25.55, 22.69, 19.65, 14.12. EIMS: m/z = 412 (M^+), 126 ($CH_3CH_2C_7H_{15}^+$). Anal. Calcd for $C_{15}H_{26}Br_2OS$: C, 43.71; H, 5.87. Found: C, 43.99; H, 5.77.

(S)-(+)-2-1-Methylpropyl p-Toluenesulfonate ((S)MPT). (*S*)MPT was synthesized from (*S*)-(+)-2-butanol using a procedure similar to that for (*S*)MOT. (*S*)MPT was obtained as colorless oil. Yield: 84.5%. $[\alpha]_{589}$: +10.25°. ^{1}H NMR ($CDCl_3$): 7.80 (d, 2H), 7.32 (d, 2H), 4.56 (m, 1H), 2.45 (s, 1H), 1.53−1.65 (m, 2H), 1.25 (m, 2H), 0.82 (t, 3H). EIMS: m/z = 228(M^+). Anal. Calcd for $C_{11}H_{16}O_3S$: C, 57.87; H, 7.06. Found: C, 57.81; H, 7.21.

3-[2-((S)-(+)-1-Methylpropyloxy)ethyl]thiophene [(S)MPET]. (*S*)MPET was synthesized from (*S*)-MPT using a method similar to that for (*S*)MOET. (*S*)MPET was obtained as pale yellow color oil. Yield: 42.2%. $[\alpha]_{589}$: −15.60°. ^{1}H NMR ($CDCl_3$): 7.24 (d, 1 H), 7.03 (s, 1 H), 6.99 (d, 1 H), 3.56−3.71 (m, 2 H), 3.34 (m, 1 H), 2.90 (t, 2 H), 1.40−1.58 (m, 2 H), 1.12 (d, 3 H), 0.88 (t, 3 H). EIMS: m/z = 184 (M^+). Anal. Calcd for $C_{10}H_{11}OS$: C, 65.17; H, 8.75. Found: C, 65.11; H, 8.70.

2,5-Dibromo-3-[2-((S)-(−)-1-methylpropyroxy)ethyl]thiophene (DBr-(S)MPET). DBr-(*S*)MPET was prepared from (*S*)MPET in a manner identical to that for DBr-(*S*)MOET. DBr-(*S*)MPET was obtained as yellow oil. Yield: 91.5%. $[\alpha]_{589}$: −8.00°. ^{1}H NMR ($CDCl_3$): 6.88 (s, 1 H), 3.50−3.71 (m, 2 H), 3.30−3.34 (m, 1 H), 2.77 (t, 2 H), 1.40−1.58 (m, 2 H), 1.12 (d, 3 H), 0.88 (t, 3 H). EIMS: m/z = 184 (M^+). Anal. Calcd for $C_{10}H_{11}Br_2OS$: C, 35.11; H, 4.12. Found: C, 35.24; H, 3.99.

Polymer Syntheses. *Head-to-Tail Poly(3-[2-((S)-(+)-1-methyloctyloxy)ethyl]thiophene) (HT-P(S)MOET).* *HT*-P(*S*)MOET was prepared using highly reactive Zn*[18] and [1,2-bis-(diphenylphosphino)ethane]dichloronickel(II) (Ni(dppe)Cl_2), as described below. DBr-(*S*)MOET (1.65 g, 4.00 mmol) was added to a THF solution of Zn* (7.30 mL) in an argon-filled drybox. The solution was kept in an ultrasonic bath at 30−35 °C for 1.5 h. Then, Ni(dppe)Cl_2 (1.10×10^{-2} g, 2.08×10^{-3} mmol) was transferred in THF (12 mL) via cannula to the reaction mixture. The mixture was refluxed for 4.5 h under argon. The polymer was precipitated using a solution of methanol and 2 M hydrochloric acid and then filtered, followed by Soxhlet purification with methanol and hexane for 3 days each. The purified polymer was dissolved in chloroform and cast on a Teflon sheet to obtain free-standing films under nitrogen. Dark purple films with a metallic luster were obtained (1.64×10^{-1} g, 16.3%). IR (ZnSe, cm^{-1}): 2958 (s, νC−H), 2920 (s, νC−H), 2851 (s, νC−H), 1516 (w, νC═C), 1466 (m, δC−H), 1372 (w, δC−H), 1341 (w, νC═C), 1138 (m, νCOC), 1091 (m, νCOC). ^{1}H NMR ($CDCl_3$): 7.09 (s, 1H), 3.64−3.76 (m, 2H), 3.44 (m, 1H), 3.07 (t, 2H), 1.55 (m, 2H), 1.25−1.41 (m, 10H), 1.12 (d, 3H), 0.85 (t, 3H). ^{13}C NMR ($CDCl_3$): 136.28, 133.51, 131.73, 129.24, 68.05, 36.70, 31.90, 30.41, 29.79, 29.34, 25.63, 22.68, 19.79, 14.11. Anal. Calcd for $(C_{15}H_{24}OS)_n$: C, 71.37; H, 9.58; S, 12.70. Found: C, 70.54; H, 10.51; S, 12.02.

Head-to-Tail Poly(3-[2-((R)-(−)-1-methyloctyloxy)ethyl]-thiophene) [HT-P(R)MOET]. *HT*-P(*R*)MOET was obtained from DBr-(*R*)MOET using a method similar to that described for *HT*-P(*S*)MOET. Yield: 10.2%. IR (ZnSe, cm^{-1}): 2958 (s, νC−H), 2925 (s, νC−H), 2854 (s, νC−H), 1516 (w, νC═C), 1466 (m, δC−H), 1372 (w, δC−H), 1341 (w, νC═C), 1138 (m, νCOC), 1091 (m, νCOC). ^{1}H NMR ($CDCl_3$): 7.09 (s, 1H), 3.64−3.74 (m, 2H), 3.44 (m, 1H), 3.06 (t, 2H), 1.57 (m, 2H), 1.24−1.41 (m, 10H), 1.12 (d, 3H), 0.85 (t, 3H). ^{13}C NMR ($CDCl_3$): 136.27, 133.50, 131.72, 129.23, 68.04, 36.70, 31.89, 30.41, 29.79, 29.34, 25.63, 22.67, 19.79, 14.11. Anal. Calcd for $(C_{15}H_{24}OS)_n$: C, 71.37; H, 9.58; S, 12.70. Found: C, 70.60; H, 10.15; S, 11.86.

Head-to-Tail Poly(3-[2-((±)-1-methyloctyloxy)ethyl]thiophene) (HT-P(±)MOET). *HT*-P(±)MOET was obtained using a method similar to that for *HT*-P(S)MOET, beginning with a mixture of DBr-(*S*)MOET and DBr-(*R*)MOET (DBr-(*S*)MOET/DBr-(*R*)MOET = 1.0:1.0 w/w) as starting materials. Yield: 12.5%. IR (ZnSe, cm^{-1}): 2958 (s, νC−H), 2924 (s, νC−H), 2854 (s, νC−H), 1510 (w, νC═C), 1456 (m, δC−H), 1373 (w, δC−H), 1340 (w, νC═C), 1138 (m, νCOC), 1093 (m, νCOC). ^{1}H NMR ($CDCl_3$): 7.10 (s, 1H), 3.63−3.80 (m, 2H), 3.44 (m, 1H), 3.07 (t, 2H), 1.57 (m, 2H), 1.17−1.41 (m, 10H), 1.12 (d, 3H), 0.85 (t, 3H). ^{13}C NMR ($CDCl_3$): 136.28, 133.51, 131.73, 129.23, 68.05, 36.71, 31.90, 30.41, 29.79, 29.36, 25.64, 22.69, 19.79, 14.12. Anal. Calcd for $(C_{15}H_{24}OS)_n$: C, 71.37; H, 9.58; S, 12.70. Found: C, 71.67; H, 9.37; S, 12.36.

Head-to-Tail Poly(3-[2-((S)-(+)-1-methylpropyloxy)ethyl]-thiophene) [HT-P(S)MPET]. *HT*-P(*R*)MPET was obtained by a method similar to that used for *HT*-P(*S*)MOET beginning with DBr-(*R*)MPET as a starting material. Yield: 29.8%. IR (ZnSe, cm^{-1}): 2965 (s, νC−H), 2923 (s, νC−H), 2870 (s, νC−H), 1508 (w, νC═C), 1451 (m, δC−H), 1373 (w, δC−H), 1340 (w, νC═C), 1135 (m, νCOC), 1084 (m, νCOC). ^{1}H NMR ($CDCl_3$): 6.88 (s, 1H), 3.50−3.71 (m, 2H), 3.30−3.34 (m, 1H), 2.77 (t, 2H), 1.40−1.58 (m, 2H), 1.12 (d, 3H), 0.88 (t, 3H). ^{13}C NMR ($CDCl_3$): 136.30, 133.51, 131.74, 129.26, 68.04, 30.40, 29.21, 19.730, 9.86. Anal. Calcd for $(C_{10}H_{14}OS)_n$: C, 65.89; H, 7.74; S, 17.59. Found: C, 65.54; H, 7.33; S, 16.47.

Preparation of Polymer Spin-Coated Films. Chloroform solutions (5 mg mL^{-1}) of polymers were prepared and filtered through a 0.5 μm filter prior to use. Spin-coated films were fabricated on quartz substrates using a MIKASA 1H-D7 spin coater at 1500 rpm for 5 s and 3000 rpm for 10 s.

Preparation of LB Films. Hydrophobic glass slides were prepared by treatment with 1,1,1,3,3,3-hexamethyl-disilazane. Chloroform solutions (0.05 mg mL^{-1}) of polymers were spread on a water subphase with a specific resistance over 17.6 Ωcm, and purified with a TORAYPURE purification system. The subphase temperature was maintained at 10 °C. The surface pressure−area (π−A) isotherm was measured on a Lauda film balance. LB films of polymers were prepared using the following procedure. The floating monolayer on pure water surface was compressed continuously up to 20 mN m^{-1}, allowing 60 min to establish the monolayer equilibrium. The monolayer on the

dx.doi.org/10.1021/la4015527 | *Langmuir* XXXX, XXX, XXX−XXX

Table 1. Molecular Weights and *HT* Ratios of *HT*-PMOETs and *HT*-P(*S*)MPET

polymer	M_n[a]	M_w[a]	M_w/M_n[a]	*HT* %[b]	band gap (E_g) /eV solution[c]	band gap (E_g) /eV solid[d]
HT-P(*S*)MOET	29 400	39 000	1.31	95.2	2.20	1.83
HT-P(*R*)MOET	28 600	35 200	1.23	95.4	2.21	1.83
HT-P(±)MOET	26 300	33 400	1.27	95.2	2.21	1.78
HT-P(*S*)MPET	19 600	29 400	1.20	92.3	2.22	1.83

[a]Determined by GPC (eluent: THF). [b]*Head-to-tail* coupling ratio determined by ^{1}H NMR. [c]Determined by band edge wavelengths of polymer chloroform solutions. [d]Determined by band edge wavelengths observed for polymer spin-coated films.

water surface then was transferred on a hydrophobic glass slide using a horizontal deposition method.

Measurements. ^{1}H and ^{13}C NMR spectra were recorded on a JEOL lambda500 spectrometer. All NMR spectra were recorded in $CDCl_3$ using tetramethylsilane (TMS) as an internal standard. FT-IR spectra were recorded using a Nicolet Magna-IR Spectrometer System 750 equipped with a liquid nitrogen cooled mercury−cadmium−telluride (MCT-A) detector. FT-IR spectra were collected for 64 scans at a resolution of 2 cm^{-1}. Molecular weights of the polymers were determined by gel permeation chromatography (GPC) using a Shimadzu LC-10AD chromatosystem equipped with Shodex KF804L columns. The eluent used was THF, which was maintained at 40 °C. A molecular weight calibration curve was obtained with standard polystyrenes. X-ray diffraction measurements of the polymer films were obtained using a Rigaku X-ray diffractometer RINT 2100 with Ni-filtered Cu−Kα radiation at 40 kV and 30 mA. The UV−Vis absorption spectra were measured on either of *HT*-PMOET and *HT*-PMPET solutions in chloroform or thin films on quartz substrates using a Shimadzu UV-3100 spectrophotometer. Specific optical rotations [α] at 589 nm were obtained using a Horiba SEPA-300 high-sensitive polarimeter at 20 °C. CD spectra of the polymer spin-coated and LS films were measured using a JASCO J-800 spectropolarimeter. In-plane conductivities were measured using the van der Pauw method at room temperature with a Keithley 2400 source meter and a Keithley 60517A electrometer.

RESULTS AND DISCUSSION

Synthesis and Characterization. The syntheses of monomers and polymers are outlined in Scheme 1. Since 3-substituted thiophene is not a symmetrical molecule, three relative orientations are available when thiophene rings are coupled between the 2- and 5-positions. The first is 2,5′ or *head-to-tail* coupling (*HT*), the second is 2,2′ or *head-to-head* coupling (*HH*), and the third is 5,5′ or *tail-to-tail* coupling (*TT*). This leads to a mixture of four chemically distinct triad regioisomers in the polymer chain when 3-substituted thiophene monomers are employed, that is, *HT-HT*, *HT-HH*, *TT-HT*, and *TT-HH* triads. These structurally irregular polymers are denoted as irregular or regiorandom. In particular, *HH* coupling is sterically unfavorable for the coplanarity of polythiophene backbones. This causes a significant loss of conjugation, which causes a loss in the desired physical properties of the material. The synthesis of regioregular *head-to-tail* poly(3-alkylthiophene)s has been accomplished using the McCullogh and Rieke method. The Rieke method has been applied for the synthesis of several 3-substituted polythiophenes because it can be conducted under mild reaction conditions at approximately 40 °C. To elucidate the structural disorder induced by the mixed regioisomers, optically active *S*-type and *R*-type poly(3-[2-(1-methyloctyloxy)ethyl]thiophene)s, *HT*-P(*S*)MOET and *HT*-P(*R*)MOET, were synthesized from 2,5-dibromo-3-[2-((*S*)-(+)-1-methyloctyloxy)ethyl] thiophene and 2,5-dibromo-3-[2-((*R*)-(−)-1-methyloctyloxy)ethyl] thiophene, respectively, using the Rieke method. For comparison, achiral poly(3-[2-(1-methyloctyloxy)ethyl]thiophene), *HT*-P(±)-MOET, also was synthesized from achiral 2,5-dibromo-3-[2-(1-methyloctyloxy)ethyl] thiophene. To investigate the effect of chain length on the optical properties, monolayer formation properties, and self-organized structure, *HT*-P(*S*)MPET, which has a shorter chain length than *HT*-P(*S*)MOET, was synthesized.

The Rieke zinc is very sensitive to moisture in the air; therefore, all procedures were conducted under an argon atmosphere. Special effort was made to keep the apparatus dry and maintain the purity of the starting dibromo monomers, DBr-MOET and DBr-MPET. Rieke zinc chemoselectively underwent direct oxidative addition with the dibromo monomers to form a 2-bromo-3-substituted-5-(bromozincio)-thiophene predominantly. The regioselectivity of this oxidative addition is a unique advantage of Zn*, providing a convenient route for the specific synthesis of regioregular organometallic reagents. Although the reaction with Zn* was indispensable to the regiospecific polymerization, the yield of 2-bromo-3-substituted-5-(bromozincio)thiophene could be low because of heterogeneous reactions. A metal surface usually is not pure. A solid coating of oxides, hydroxides, and carbonates constitutes a "passivation" layer that can prevent reagents in solution from reaching the metal. Ultrasonic irradiation has been used to facilitate heterogeneous reactions by removing surface absorbed contaminants.[35,36] Using an ultrasonication treatment was expected to activate the surface of Zn* and increase its catalytic activity. Therefore, ultrasonication treatment was used to activate the zinc.

After precipitation from the reaction solution using methanol, *HT*-PMOET was Soxhlet-extracted with hexane, followed by extraction with chloroform. The GPC results indicated that the *HT*-PMOET extracted with hexane had a lower molecular weight than that extracted with chloroform, therefore chloroform-extracted *HT*-PMOET was used for the following experiments. The *HT*-PMOET and *HT*-PMPET obtained were reddish brown with a metallic luster, and were readily soluble in $CHCl_3$ and THF.

Table 1 shows the number-average molecular weight M_n, weight-average molecular weight M_w, and polydispersity index $Đ_M = M_w/M_n$ of the polymers synthesized in this study. The molecular weight of *HT*-PMOET was 26.3−29.4 kg mol^{-1} with a narrow weight distribution of 1.23−1.31. The molecular weight of *HT*-P(*S*)MPET was 19.6 kg mol^{-1}, which was lower than that of *HT*-PMOET. The number of monomer units per single chain for *HT*-PMOET was in the range of 104−116, and that for *HT*-P(*S*)MPET was 107. Note that the numbers of monomer units of the polymers were nearly equal, allowing comparison of their properties. Regioregularity of the polymers was estimated by ^{1}H NMR in $CDCl_3$. The ^{1}H NMR spectrum of poly(3-substituted thiophene) provided sensitive probes for the substitution pattern in the polymer backbone. The α-

dx.doi.org/10.1021/la4015527 | *Langmuir* XXXX, XXX, XXX−XXX

methylene protons of the thiophene ring produced two signals because of the regioisomers. In the ^{1}H NMR spectrum, the downfield signal was assigned to a *head-to-tail* coupled dyad (δ = 3.07) and the upfield signal was assigned to a *head-to-head* coupled dyad (δ = 2.83). The *head-to-tail* ratio of *HT*-PMOET and *HT*-P(*S*)MPET, as estimated from the α-methylene signal (Figure S1, Supporting Information), indicated greater than 92% *head-to-tail*, which was nearly equal to the ratios found for conventional poly(3-alkylthiophene)s obtained by the Rieke method.[32]

Optical Properties and Structural Analyses of Polymers. A qualitative measure of π-orbital overlap in solution can be obtained using UV−vis absorption spectroscopy. In conjugated polymers, the extent of conjugation length directly affects the observed energy of the absorption. Therefore, UV−vis spectroscopy can be used to observe the conformational state and structure of π-conjugated polymers. An increase in the maximum absorption wavelength (λ_{max}) is evidence for increased coplanarity and longer π-conjugation length. Figure 1 shows the UV−vis absorption spectra of chiral *HT*-PMOET

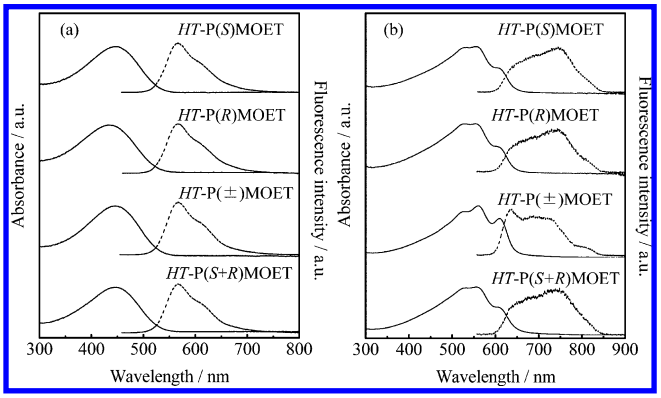

Figure 1. UV−vis absorption (solid line) and fluorescence (dotted line) spectra of (a) $CHCl_3$ solutions and (b) spin-coated films of *HT*-PMOETs. The excitation wavelength was equal to the absorption maximum (λ_{max}) of each polymer.

in $CHCl_3$ and spin-coated films. For comparison, optical absorption spectra of racemic polymer *HT*-P(±)MOET and a mixture of *HT*-P(*S*)MOET and *HT*-P(*R*)MOET (50:50 w/w; *HT*-P(*S*+*R*)MOET) are displayed in Figure 1. All of the polymer solutions produced similar absorption spectra with a maximum absorption peak at approximately 446 nm, assigned to the $\pi-\pi^*$ transition of the conjugated polymer backbone. The side-chain chirality did not cause any significant changes in the UV−Vis absorption spectra in the solution state. From the onset of absorption observed near 600 nm, the band gap (E_g) in solution was estimated to be approximately 2.2 eV for all polymers, as shown in Table 1. The *HT*-PMOET spin-coated films prepared from a chloroform solution exhibited distinct three absorption peaks; the absorption maximum at 577 nm, the lower-intensity peak appear at 608 nm, and a shoulder at 529 nm. The lowest energy peak at 608 nm was attributed to the exciton band, and the higher energy peak was assigned to vinronic sidebands.[37] The absorption edge of the film was approximately 780 nm (1.59 eV), which was about 200 nm red-shifted from that of the chloroform solution. This indicates that *HT*-PMOET possesses a more planar conformation in the solid film compared with that in solution. These results were consistent with the optical properties of typical poly(3-alkylthiophene)s, which produced a significant red shift between solution and solid film.[18] Racemic polymer, *HT*-P(±)MOET, showed relatively sharp peaks compared with other *HT*-PMOETs, suggesting that *HT*-P(±)MOET formed stable $\pi-\pi$ stacking. This is probably due to the loss of homochiral interactions. The chiral discrimination phenomenon arises from a nonequivalence in the interaction potential between two molecules of the same chirality (*S*:*S*) versus that between two molecules of opposite chirality (*S*:*R*). If the *S*:*S* and *R*:*R* interactions are more favorable than the *S*:*R* interaction, homochiral discrimination is indicated, while a more favorable *S*:*R* interaction indicates heterochiral discrimination. These results indicate that the $\pi-\pi$ stacking was affected by chiral interactions and exhibited heterochiral behavior. For similar reasons, the band gap value of racemic *HT*-P(±)MOET was less than that of chiral *HT*-PMOET, as shown in Table 1. The *HT*-PMOET showed fluorescence in $CHCl_3$ and spin-coated films. In $CHCl_3$ solutions, similar fluorescence spectra were observed for all *HT*-PMOETs. However, the fluorescence spectra of *HT*-PMOET in the solid state were affected by the presence of chirality. *HT*-P(*S*)MOET, *HT*-P(*R*)MOET, and their mixture *HT*-P(*S*+*R*)MOET spin-coated films showed a fluorescence peak at 740 nm, and *HT*-P(±)MOET showed a fluorescence peak at 635 nm, with shoulders at 696 and 808 nm.

HT-P(*S*)MPET with a shorter chain length than *HT*-P(*S*)MOET showed an absorption peak at 443 nm owing to the $\pi-\pi^*$ transition, and a fluorescence peak at 567 nm in $CHCl_3$ solution (Figure S2, Supporting Information). These spectra were similar to those of *HT*-P(*S*)MOET. For a spin-coated film, absorption peaks were observed at 524 and 555 nm, with a shoulder at 613 nm, and sharp fluorescence peaks were observed at 648 and 714 nm. These results indicate that the optical properties were independent of chain length. The fluorescence intensity of *HT*-P(*S*)MPET was greater than that of *HT*-P(*S*)MOET.

The self-organization properties of the chiral polythiophenes were examined using X-ray diffraction. Figure 2 shows X-ray

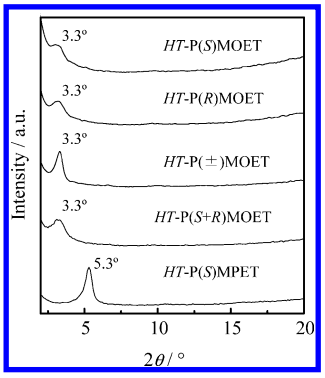

Figure 2. X-ray diffraction patterns of *HT*-PMOETs and *HT*-PMPET cast films.

diffraction patterns of the polymer cast films. The Bragg reflection was observed at a 2θ angle of 3.3° for *HT*-PMOET and at 5.3° for *HT*-P(*S*)MPET. These peaks corresponded to the interlayer *d*-spacings of 26.7 Å for *HT*-PMOET and 16.7 Å for *HT*-PMPET, which are the stacking distances between two polymer main chains. These results showed that the regioregular *HT*-PMOET and *HT*-PMPET possessed self-assembling tendencies to form a highly ordered and crystalline

dx.doi.org/10.1021/la4015527 | *Langmuir* XXXX, XXX, XXX−XXX

structure. Peak intensity and sharpness of *HT*-P(*S*)MPET were greater than those of *HT*-P(*S*)MOET, suggesting that the crystallinity of *HT*-P(*S*)MPET was greater than that of *HT*-P(*S*)MOET. The X-ray diffraction peak observed for racemic *HT*-P(±)MOET was sharper than that of other *HT*-PMOETs, suggesting that *HT*-P(±)MOET has a more crystalline structure. The chiral substituents twist the polymer main chains; thus, the interaction between the polymer main chains of chiral polythiophenes was weakened compared to that of achiral polymers. For *HT*-P(*R*+*S*)MOET, because the homochiral organization was preferred, phenomena similar to those exhibited by *HT*-P(*S*)MOET and *HT*-P(*R*)MOET were observed.

HT-P(*S*)MOET showed clear solvatochromism upon adding methanol as a poor solvent (Figure S2, Supporting Information). The maximum absorption peak of *HT*-P(*S*)-MOET red-shifted upon varying the mixture ratio of $CHCl_3$ and MeOH. The absorption spectra for a 1:4 (*v*/*v*) $CHCl_3$/MeOH solution was similar to that of the *HT*-P(*S*)MOET spin-coated films, indicating that the polymer chains are self-organized to form an aggregated phase. While no CD effect was observed in $CHCl_3$, bisignate Cotton effects were clearly observed for 2:3 and 1:4 (v/v) chloroform/methanol solutions, as shown in Figure SI1 (Supporting Information). Strong positive Cotton effects for *HT*-P(*S*)MOET were observed at about 570 and 610 nm, and negative Cotton effects were observed at about 490 nm in 1:4 (v/v) $CHCl_3$/MeOH solution. The presence of a CD effect in the $\pi-\pi^*$ transition region shows that the side chain chirality induced optical activity in the poly(thiophene) main chains. Consequently, the bisignate Cotton effects suggested that the conjugated unit of *HT*-P(*S*)MOET was self-organized to array clockwise along the main chain, or that their main chains stacked in a twisted form, according to exciton chirality theory.[38]

Figure 3 shows CD spectra of the *HT*-PMOET and *HT*-P(*S*)MPET spin-coated films. Racemic *HT*-P(±)MOET and the mixture *HT*-P(*R*+*S*)MOET films showed no circular dichroism. Strong positive or negative Cotton effects in the

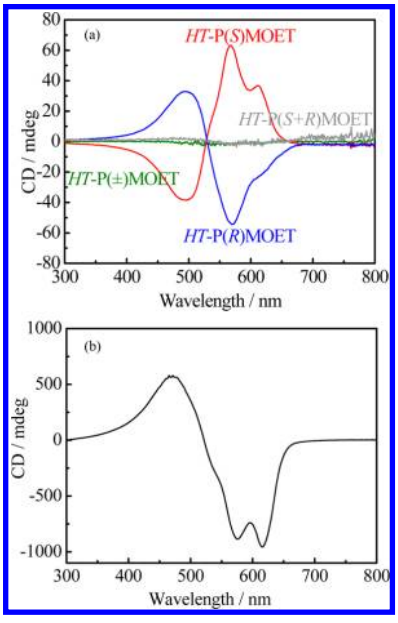

Figure 3. CD spectra of (a) *HT*-PMOET and (b) *HT*-P(S)MPET spin-coated films.

$\pi-\pi^*$ absorption region of the conjugated main chains were observed for the chiral polymers in the solid state. For *HT*-P(*S*)MOET, strong positive Cotton effects were observed at about 570 and 610 nm and negative Cotton effects at about 490 nm, which were consistent with the 1:4 (v/v) $CHCl_3$/MeOH solution, as shown in Figure 3b. This result indicates that the chiral polymer forms the same aggregated structure in mixed solution and in film. For *HT*-P(*R*)MOET, inversed CD spectra for *HT*-P(*S*)MOET were observed, indicating that *HT*-P(*R*)MOET forms a counterclockwise array. *HT*-P(*S*)MPET also showed a strong CD effect in the solid state (Figure 3b). For *HT*-P(*S*)MPET, negative Cotton effects were observed at about 575 and 615 nm and negative Cotton effects at about 469 nm. Shortening the side chain length of the chiral side chain inversed the helicity and dramatically increased CD intensity. These results indicate that *HT*-P(*S*)MPET had a favorable side chain length for forming chiral morphology.

Monolayer Formation of Polymers at the Air–Water Interface and Fabrication of Ultrathin Multilayers. Ultrathin films have attracted attention because of their potential as a novel class of materials. To realize the maximum potential of polymeric materials, the structure–property relationships must be well understood. Ultrathin films are useful not only for technological applications but also for scientific investigations. The LB technique is considered the most suitable for ultrathin film fabrication with specific structures planned at the molecular level. Interest has increased recently in the preparation of conducting polymer multilayer films from functional organic compounds. A previous study reported that chiral poly(3-substituted thiophene), *head-to-tail* poly(3-{2-{(S)-2-methylbutoxy}ethyl}thiophene, *HT*-P(*S*)-MBET, with ether groups in the side chains, can form a stable monolayer at the air–water interface without the need for supporting materials such as stearic acid.[33] Because *HT*-PMOET has a longer side chain, which is effective for monolayer formation, monolayer stability and film forming ability were investigated.

Chloroform solutions of the polythiophene derivatives were spread on the water surface of a Lauda trough. Figure 4 shows

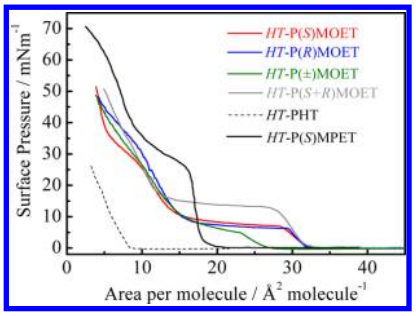

Figure 4. $\pi-A$ isotherms of *HT*-PMOETs, *HT*-P(S)MPET, and *HT*-PHT monolayers on pure water at 10 °C.

the pressure–area ($\pi-A$) isotherms of *HT*-P(*S*)MOET, *HT*-P(*R*)MOET, *HT*-P(*S*+*R*)MOET, *HT*-P(±)MOET, and *HT*-P(*S*)MPET for the compression process at a subphase temperature of 10 °C. The horizontal axis indicates the molecular area per thiophene unit. For comparison, the π-A isotherm of *head-to-tail* poly(hexythiophene) (*HT*-PHT), which is a hydrophobic polymer, is shown. For nonamphiphilic *HT*-PHT, the surface pressure began to increase at 9.3 $Å^2$, and increased up to 20 mN m^{-1}, indicating that an ideal spread

dx.doi.org/10.1021/la4015527 | *Langmuir* XXXX, XXX, XXX–XXX

monolayer did not form, because the molecular area was considerably smaller than the estimated value. In contrast, π–A isotherms of *HT*-PMOET and *HT*-P(*S*)MPET showed a relatively smooth rise in pressure at a large molecular area. This is because of the existence of hydrophilic ether groups in the side chains. By compressing the *HT*-PMOET and *HT*-P(*S*)MPET monolayers on the water surface, a phase transition was observed at a specific surface pressure that depended on the polymer. After the pressure reached the transition point, the surface pressure remained constant as the area decreased. The pressure rose again when the area per molecule reached that of a pure condensed polythiophene monolayer. Table 2 shows the limiting area per repeat unit of *HT*-PMOET and *HT*-P(*S*)MPET before and after phase transition. Here the limiting area per molecule was determined by extrapolating the area from the isotherm to pressure π = 0.

Table 2. Area per molecule of *HT*-PMOETs and *HT*-P(S)MPET monolayers at the air–water interface before and after transition pressure at 10 °C

	area per molecule/Å^2 molecule^{-1}	
polymer	before transition	after transition
HT-P(*S*)MOET	34	18
HT-P(*R*)MOET	33	18
HT-P(±)MOET	28	20
HT-P(*S*+*R*)MOET	34	18
HT P(*S*)MPET	19	16
HT P(*S*)MBET	17[a]	14[a]

[a]Reference 33.

The effect of chiral interactions on monolayer formation of *HT*-PMOET was studied. For *HT*-PMOET, the limiting area per molecule before phase transition was 33–34 Å^2 molecule^{-1} for *HT*-P(*S*)MOET, *HT*-P(*R*)MOET, and *HT*-P(*S*+*R*)MOET. According to the Corey–Pauling–Koltun (CPK) molecular models, these values correspond to the cross section of the thiophene ring and alkoxy side chains, as shown in Figure 5. For *HT*-P(±)MOET, the limiting area per molecule was 28 Å^2, which was smaller than that of other *HT*-PMOETs. While chiral polythiophene expanded on the water surface because of chiral repulsion and steric distortion, racemic polythiophene showed a stronger packing nature because of the achiral side chains. As the monolayer was compressed, a phase transition was observed at 7.1 mN m^{-1} for *HT*-P(*S*)MOET, *HT*-P(*R*)MOET, and *HT*-P(±)MOET, and at 15.0 mN m^{-1} for *HT*-P(*S*+*R*)MOET. The surface pressure remained constant with decreasing area at the transition point, and then the pressure began to rise as the limiting area reached approximately 18 Å^2 molecule^{-1}, as shown in Table 2. According to the CPK molecular models, these values correspond to the cross section of the thiophene ring of *HT*-PMOET. The most probable molecular orientation involves

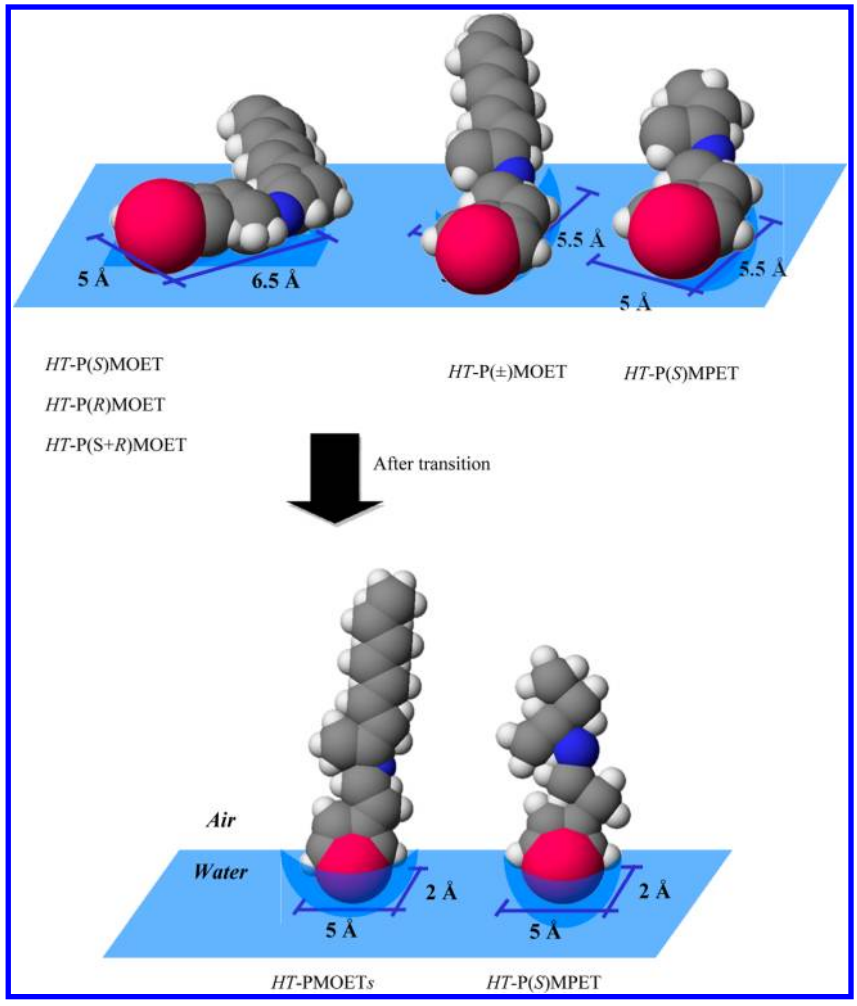

Figure 5. CPK models of *HT*-PMOETs and *HT*-P(*S*)MPET at the air–water interface before and after transition.

dx.doi.org/10.1021/la4015527 | *Langmuir* XXXX, XXX, XXX–XXX

coplanar polythiophene backbones that float on the water surface and side chains on one side of the zigzag formation orient toward the water phase.

Next, the effect of side chain length on monolayer formation was investigated. The monolayer of *HT*-P(*S*)MPET showed a steep rise at 19 Å^2, which is smaller than that of *HT*-P(*S*)MOET, with a phase transition at 25 mN m^{-1}, which is higher than that of *HT*-P(*S*)MOET. According to the CPK molecular models, this molecular area corresponds to the cross section of the thiophene ring of *HT*-PMOET. Because the length of the hydrophobic portion of the side chain of *HT*-P(*S*)MPET was shorter than that of *HT*-P(*S*)MOET, the amphiphilic balance in the polythiophene, which affects monolayer spread behavior, was affected. Compared with chiral polythiophene, *HT*-P(*S*)MEBT and *HT*-P(*S*)MOET form stable monolayers on the water surface.

Multilayer Formation of *HT*-PMOET and *HT*-P(*S*)MPET. Layer-by-layer multilayer deposition was attempted by repeated horizontal deposition procedures at a pressure 20 mN m^{-1} and temperature of 10 °C. UV−vis absorption spectra of the layer-by-layer deposited films of *HT*-P(*S*)MOET are shown in Figure 6. *HT*-P(*S*)MOET LB films showed absorption peaks at 564

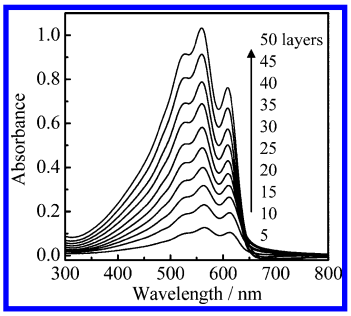

Figure 6. UV−vis absorption spectra of *HT*-P(S)MOET multilayer films transferred on a glass substrate. The transfer was performed at 20 mN m^{-1} by repeating the horizontal deposition sequence for up to 50 cycles.

and 614 nm, with shoulders at 480 and 528 nm, increasing the deposition number. The maximum absorption peak of the LB films showed a lower $\pi-\pi^*$ transition energy than that of the spin-coated films, while the intensity of the shoulder peak near 610 nm was relatively stronger than that of the spin-coated film. These results suggest that the *HT*-P(*S*)MOET molecules in the LB films tend to form a more planar conformation with longer conjugation length compared to those in spin-coated films. Similar results were observed for other *HT*-PMOETs and *HT*-P(*S*)MPETs. Figure 7 shows X-ray diffraction patterns of the 50-layer multilayer films of *HT*-PMOET and *HT*-P(*S*)MPET. Diffraction patterns were observed for all LB films. More intense and sharper peaks were observed for *HT*-PMOET LB film than for *HT*-PMOET spin-coated films. Thus, the LB technique provides molecular control over regioregular polymers for forming more organized structures that exhibit more planar conformations. In contrast, the X-ray diffraction peak of the *HT*-P(*S*)MOET LB films was broad and weak compared with spin-coated films. The short side chains of *HT*-P(*S*)MOET are not favorable for constructing organized structures using the LB method.

Chiroptical and Electrical Properties of LB Films. Figure 8 shows the CD spectra of the 50-layer multilayer films of *HT*-PMOET and *HT*-P(*S*)MPET. Chiral *HT*-P(*S*)MOET

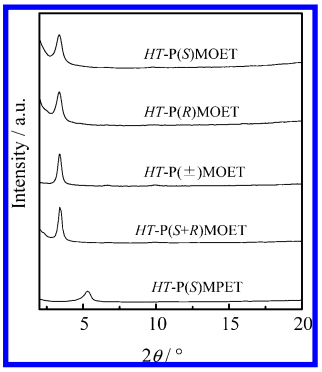

Figure 7. X-ray diffraction patterns of *HT*-PMOETs and *HT*-P(*S*)MPET LB films with 50 layers.

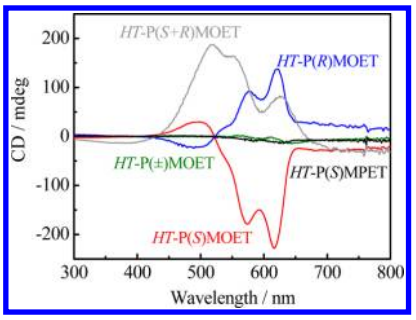

Figure 8. CD spectra of *HT*-PMOETs and *HT*-P(*S*)MPET LB films with 50 layers.

and *HT*-P(*R*)MOET LB films showed strong positive and negative Cotton effects, respectively, in the $\pi-\pi^*$ absorption region of the conjugated main chains, while *HT*-P(±)MOET LB films did not produce a CD signal. The CD intensities of *HT*-P(*S*)MOET and *HT*-P(*R*)MOET LB films were much greater than those of their spin-coated films. The presence of stronger CD signals show that the highly organized polymer structure formed by spreading on the water surface enhanced the chirality of the poly(thiophene) main chains. In addition, CD signals of the LB films were inverse compared to those of the spin-coated films. Using the horizontal dipping method, polymer films were transferred upside down on the substrate; the LB films obtained showed CD signals with a reverse sign. Surprisingly, *HT*-P(*S*+*R*)MOET produced CD signals that were not identical to those of chiral *HT*-P(*S*)MOET and *HT*-P(*R*)MOET. *HT*-P(*S*)MPET produced no CD signal for two main reasons: the strong packing interactions between main chains owing to small repulsions between side chains, and the lower transfer pressure compared to the transition pressure of *HT*-P(*S*)MPET that optimized chiral conformation.

Electrical conductivity of the polymer spin-coated and LB films was measured using the van der Pauw method.[39] Chemical doping of polymers was performed by dipping the polymer films for a specified time into acetonitrile containing $FeCl_3$ as a dopant. Doping was accompanied by an obvious color change from red to bluish purple. The UV−vis absorption spectra provided valuable information about the level of oxidation achieved by various doping processes. After doping, absorption bands for the polythiophene conjugated backbone disappeared at about 530 nm and new lower energy bands centered at about 860 and 2500 nm appeared. These bands are characteristic of a highly oxidized conjugated backbone, that is, supporting localized defect states in the form of bipolarons.

dx.doi.org/10.1021/la4015527 | *Langmuir* XXXX, XXX, XXX−XXX

Significant reductions in the interband $\pi-\pi^*$ transition region were observed for all polymer spin-coated and LB films. Table 3 shows the in-plane conductivity of the polymer spin-coated and LB films before and after doping with $FeCl_3$. The in-plane conductivities of the neutral *HT*-PMOET and *HT*-PMPET spin-coated films were on the order of 10^{-5} Scm^{-1}, whereas those of the neutral LB films with 20 layers were on the order of 10^{-4} Scm^{-1}. After being doped with $FeCl_3$, the in-plane conductivities of both spin-coated and LB films were enhanced dramatically. The in-plane conductivities of the doped *HT*-PMOET and *HT*-PMPET spin-coated films were on the order of 10^{-1} Scm^{-1}, whereas the conductivities of the *HT*-PMOET and *HT*-PMPET LB films were 0.5−6 S cm^{-1}. This suggests that the LB manipulation induced self-organized properties in *HT*-PMOET and *HT*-P(*S*)MPET molecules and extended their conjugation length. While differences between *S*, *R*, and racemic *HT*-PMOET were not observed, *HT*-P(*S*+*R*)MOET LB films showed relatively low electrical conductivity.

Table 3. Conductivity of Prepared and Doped Polymer Films As Measured by the van der Pauw Method

		conductivity/S cm^{-1}	
polymer	preparation method	as prepared	doped[a]
HT-P(*S*)MOET	spin-coat	6.6×10^{-5}	1.9×10^{-1}
	LS	2.9×10^{-4}	2.1
HT-P(*R*)MOET	spin-coat	8.8×10^{-5}	1.7×10^{-1}
	LS	2.8×10^{-4}	1.3
HT-P(±)MOET	spin-coat	6.6×10^{-5}	2.2×10^{-1}
	LS	2.9×10^{-4}	1.6
HT-P(*S*+*R*)MOET	spin-coat	4.0×10^{-5}	2.2×10^{-1}
	LS	1.8×10^{-4}	5.0×10^{-1}
HT P(*S*)MPET	spin-coat	1.1×10^{-5}	5.0×10^{-1}
	LS	1.2×10^{-4}	6.0

[a]Chemical doping was performed by dipping polymer films in 2 mg mL^{-1} $FeCl_3$ acetonitrile solution for 10 min.

CONCLUSIONS

The synthesis and LB film formation of regioregular chiral polythiophenes were investigated, and the effects of chirality and side chain structure on the electrical and optical properties of polythiophenes were determined. Regioregular chiral (*S*- and *R*-) and achiral *HT*-PMOET and chiral *HT*-PMPET (*S*-type) with greater than 92% *head-to-tail* coupling were synthesized using the Rieke method. X-ray diffraction patterns of the cast films indicated that *HT*-PMOET and *HT*-PMPET possessed a well-organized lamellar structure, with a decrease in crystallinity upon introduction of chirality and side chain extension. Chiral *HT*-PMOET spin-coated films and aggregated state in solution exhibited circular dichroism in the $\pi-\pi^*$ transition region. The presence of a CD effect indicates that side chain chirality induced optical activity in poly(thiophene) main chains. *HT*-PMOET and *HT*-PMPET formed stable monolayers on the water surface to produce highly electrically conductive and chiral LB films. The introduction of suitable functional groups and application of LB method can improve molecular organization, which can also provide materials with excellent optical and electrical properties.

ASSOCIATED CONTENT

Supporting Information

^1H NMR, UV−vis absorption spectra, CD spectra of polymers; UV−vis-NIR spectra of polymer spin-coated films after $FeCl_3$ doping. This material is available free of charge via the Internet at http://pubs.acs.org

AUTHOR INFORMATION

Corresponding Author

*E-mail: y-tabuch@sophia.ac.jp (Y.T.); m-rikuka@sophia.ac.jp (M.R.).

Notes

The authors declare no competing financial interest.

REFERENCES

(1) Perepichka, I. F., Perepichka, D. F., Eds. *Handbook of Thiophene-based Materials*; Wiley: Chichester, 2009.
(2) Angelopoulus, M. In *Handbook of Conducting Polymers*, 2nd ed.; Sktheim, T. A., Elsenbaumer, R. L., Reynolds, J. R., Eds.; Marcel Dekker: New York, 1998; Chapter 32, pp 921−944.
(3) Andersson, M. R.; Inganas, O.; Gustafsson, G.; Gustafsson-Carlberg, J. C.; Selse, D.; Hjertberg, T.; Wennerstrom, O. Electrluminescence from substituted poly(thiophenes): From blue to near-infrared. *Macromolecules* **1995**, *28*, 7525−7529.
(4) Barta, P.; Cacialli, F.; Friend, R. H.; Zagórska, M. Efficient photo and electroluminescence of regioregular poly(alkylthiophene)s. *J. Appl. Phys.* **1998**, *84*, 6279−6284.
(5) Ahn, S.-H.; Czae, M.-Z.; Kim, E.-R.; Lee, H.; Han, S.-H.; Noh, J.; Hara, M. Synthesis and characterization of soluble polythiophene derivatives containing electro-transporting moiety. *Macromolecules* **2001**, *34*, 2522−2527.
(6) Cheylan, S.; Bolink, H. G.; Fraleoni-Morgera, A.; Puigdollers, J.; Voz, C.; Mencarelli, I.; Setti, L.; Alcubilla, R.; Badenes, G. Improving the efficiency of light-emmiting diode based on a thiophene polymer containing a cyano group. *Org. Electron.* **2007**, *8*, 641−647.
(7) Roman, L.; Mammo, W.; Petterson, L.; Andersson, M.; Inganas, O. High quantum efficiency polythiophene. *Adv. Mater.* **1998**, *10*, 774−777.
(8) Cheng, Y. J.; Yang, S. H.; Hsu, C. S. Synthesis of conjugated polymers for organic solar cell applications. *Chem. Rev.* **2009**, *109*, 5868−5923.
(9) Kaneto, K.; Lim, W. Y.; Takashima, W.; Endo, T.; Rikukawa, M. Alkyl chain length dependence of field-effect moblities in regioregular poly(3-alkylthiophene) films. *Jpn. J. Appl. Phys., Part 2* **2000**, *39*, L872−L874.
(10) Sirringhaus, H.; Brown, P. J.; Friend, R. H.; Nielsen, M. M.; Bechgaard, K.; Lngeveld-Voss, B. M. W.; Spiering, A. J. H.; Janssen, R. A. J.; Meijer, E. W.; Herwig, P.; de Leeuw, D. W. Two-dimensional charge transport in self-organized, high-mobility conjugated polymers. *Nature* **1999**, *401*, 685−688.
(11) Ong, B. S.; Wu, Y.; Liu, P.; Gardner, S. High-performance semiconducting polythiophenes for organic thin-film transistors. *J. Am. Chem. Soc.* **2004**, *126*, 3378−3379.
(12) Thomas, S. W.; Joly, G. D.; Swager, T. M. Cemical sensors based on amplifying fluorescent conjugated polymers. *Chem. Rev.* **2007**, *107*, 1339−1386.
(13) Hirahara, T.; Yoshizawa-Fujita, M.; Takeoka, Y.; Rikukawa, M. Highly efficient circular polarized light emission in the green region from chiral polyfluorene-thiophene thin films. *Chem. Lett.* **2012**, *41* (9), 905−907.
(14) Hirahara, T.; Yoshizawa-Fujita, M.; Takeoka, Y.; Rikukawa, M. Optical properties of polyfluorene-polythiophene copolymers having chiral side chains. *Synth. Met.* **2009**, *159*, 2180.
(15) Kane-Maquire, L. A. P.; Wallace, G. G. Chiral conducting polymers. *Chem. Soc. Rev.* **2010**, *39*, 2545−2576.

dx.doi.org/10.1021/la4015527 | *Langmuir* XXXX, XXX, XXX−XXX

(16) Cornelissen, J. J. L. M.; Rowan, A. E.; Nolte, R. J. M.; Sommerdijk, N. A. J. M. Chiral architectures from macromolecular building blocks. *Chem. Rev.* **2001**, *101*, 4039−4070.
(17) Matsushita, S.; Jeong, Y. S.; Akagi, K. Electrochromism-driven linearly circularly polarized dichroism of poly(3,4-ethylenedioxythiophene) derivatives with chirality and liquid crystallinity. *Chem. Commun.* **2013**, *49*, 1883−1890.
(18) Chen, T.-A.; Wu, X.; Rieke, R. D. Regiocontrolled synthesis of poly(3-alkylthiophenes) mediated by Rieke zinc: Their characterization and solid-state properties. *J. Am. Chem. Soc.* **1995**, *117*, 233−244.
(19) McCullough, R. D.; Lowe, R. D.; Jayaraman, M.; Anderson, D. L. Design, synthesis, and control of conducting polymer architectures: structurally homogeneous poly(3-alkylthiophenes). *J. Org. Chem.* **1993**, *58*, 904−912.
(20) Pandey, S. S.; Takashima, W.; Nagamatsu, S.; Endo, T.; Rikukawa, M.; Kaneto, K. Regioregularity vs regiorandomness: Effect on photocarrier transport in poly(3-hexylthiophene). *Jpn. J. Appl. Phys., Part 2* **2000**, *39*, L94−L97.
(21) Takeoka, Y.; Iguchi, Y.; Rikukawa, M.; Sanui, K. Self-assembled multilayer films based on functionalized poly(thiophene)s. *Synth. Met.* **2005**, *153*, 121−124.
(22) Xu, G. F.; Bao, Z. N.; Groves, J. T. Langmuir−Blodgett films of regioregular poly(3-hexylthiophene) as field-effect transistors. *Langmuir* **2000**, *16*, 1834−1841.
(23) Bao, Z.; Dodabalapur, A.; Lovinger, A. Soluble and processable regioregular poly(3-hexylthiophene) for thin film transistor applications with high mobility. *J. Appl. Phys. Lett.* **1996**, *69*, 4108−4110.
(24) Watanabe, I.; Hong, K.; Rubner, M. F. Langmuir-Blodgett manipulation of poly(3-alkylthiophenes). *Langmuir* **1990**, *6*, 1164−1172.
(25) Ahlskog, M.; Paloheimo, J.; Stubb, H.; Dyreklev, P.; Fahlman, M.; Inganäs, O.; Andersson, M. R. Thermochromism and optical absorption in Langmuir-Blodgett films of alkyl-substituted polythiophenes. *J. Appl. Phys.* **1994**, *76*, 893−899.
(26) Hassenkam, T.; Greve, D. R.; Björnholm, T. Direct visualization of nanoscale morphology of conducting polythiophene monolayers studied by electrostatic force microscopy. *Adv. Mater.* **2001**, *13*, 631−634.
(27) Björnholm, T.; Hassenkam, T.; Reitzel, N. Supramolecular organization of highly conducting organicthin films by the Langmuir-Blodgett techniques. *J. Mater. Chem.* **1999**, *9*, 1975−1990.
(28) Ulman, A. *An Introduction to Ultrathin Organic Films: From Langmuir−Blodgett to Self-Assembly*; Academic Press: Boston, 1991.
(29) Ochiai, K.; Tabuchi, Y.; Rikukawa, M.; Sanui, K. Fabrication of chiral poly(thiophene) Langmuir-Blodgett films. *Thin Solid Films* **1998**, *327*, 454−457.
(30) Nagano, S.; Kodama, S.; Seki, T. Ideal spread monolayer and multilayer formation of fully hydrophobic polythiophenes via liquid crystal hybridization on water. *Langmuir* **2008**, *24*, 10498−10504.
(31) Rikukawa, M.; Nakagawa, M.; Ishida, K.; Be, H.; Sanui, K.; Ogata, N. Electrical properties of conductive Languir-Blodgett films comprised of head-to-tail poly(3-hexylthiophehe). *Thin Solid Films* **1996**, *284*, 636−639.
(32) Rikukawa, M.; Nakagawa, M.; Tabuchi, Y.; Sanui, K.; Ogata, N. Self-organization and electrical properties of head-to-tail poly(3-hexylthiophene) in Langmuir-Blodgett films. *Synth. Met.* **1997**, *84*, 233−234.
(33) Ochiai, K.; Rikukawa, M.; Sanui, K. Novel highly ordered Langmuir-Blodgett films of regioregular poly(3-substituted thiophene). *Chem. Commun.* **1999**, 867−868.
(34) Saito, F.; Takeoka, Y.; Rikukawa, M.; Sanui, K. Synthesis of optically active regioregular poly(thiophene). *Synth. Met.* **2005**, *153*, 125−128.
(35) Boudjouk, P.; Han, B.-H.; Anderson, K. R. Sonochemical and electrochemical synthesis of tetramesityldisilene. *J. Am. Chem. Soc.* **1982**, *104*, 4992−4993.
(36) Gilman, H.; Vanderwal, R. J. Some incidental factors affecting the starting of gignard reagents. *Recl. Trav. Chim. Pays-Bass* **1929**, *48*, 160−162.
(37) Kishino, S.; Ueno, Y.; Ochiai, K.; Rikukawa, M.; Sanui, K.; Kobayashi, T.; Kunugita, H.; Ema, K. Estimate of the effective conjugation length of polythiophene from its $|\chi^{(3)}(\omega;\omega,\omega,-\omega)|$ spectrum at excitonic resonance. *Phys. Rev. B* **1998**, *58*, 13430−13433.
(38) Berove, N.; Nakanishi, K.; Woody, R. W. *Circular Dichroism: Principles and Applications*, 2nd ed.; Wiley-VCH: New York, 2000.
(39) Pauw, V. D. A method of measuring specific resistivity and Hall effect of discs of arbitrary shape. *Philips Res. Rep.* **1958**, *13*, 1−9.

dx.doi.org/10.1021/la4015527 | *Langmuir* XXXX, XXX, XXX−XXX